ACS APPLIED MATERIALS & INTERFACES

Research Article

www.acsami.org

Three-Dimensional Highly Conductive Graphene–Silver Nanowire Hybrid Foams for Flexible and Stretchable Conductors

Chao Wu,[†] Lijun Fang,[†] Xingyi Huang,* and Pingkai Jiang*

Department of Polymer Science and Engineering, Shanghai Key Lab of Electrical Insulation and Thermal Aging, Shanghai Jiao Tong University, 800 Dongchuan Road, Shanghai 200240, P. R. China

Supporting Information

ABSTRACT: Graphene foams have showed huge application potentials owing to their unique 3D structure and superior properties. Thus, it is highly desired to develop a simple and effective pathway to fabricate high performance graphene-based foams. Here, we present a polymer template-assisted assembly strategy for fabricating a novel class of graphene/AgNW hybrid foams. The hybrid foams show 3D ordered microstructures, high thermal stability, and excellent electrical and mechanical properties, and demonstrate huge application potential in the fields of flexible and stretchable conductors. Importantly, the polymer-template assisted assembly technique is simple, scalable, and low-cost, providing a new synthesis protocol for various multifunctional graphene hybrid foam-based composites.

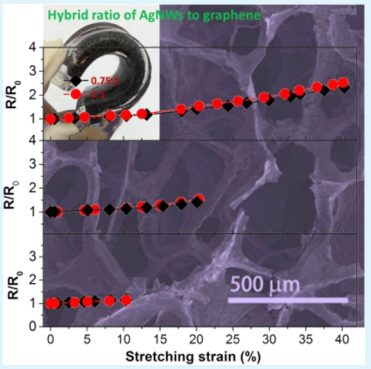

KEYWORDS: *graphene, silver nanowires, hybrid foams, flexible conductors, assembly*

INTRODUCTION

Graphene foams, three-dimensional (3D) interconnected graphene networks, have gained great attention recently owing to their unique structure and superior physical properties such as high overall electrical conductivity,[1,2] large specific surface area,[3,4] excellent mechanical flexibility,[5,6] and high thermal and chemical stability.[7] Such structure and fascinating properties render graphene foams huge application potentials in the fields of energy storage such as supercapacitors and lithium-ion battery electrodes,[8−11] flexible conductors,[1,2,12] electromagnetic shielding,[13] as well as oil cleanup.[14−16] To harness graphene foams for these applications, several approaches have been developed for the fabrication of graphene foams, mainly including hydrothermal reduction of graphene oxides (GOs),[8,17] chemical reduction of GO,[18−20] and chemical vapor deposition (CVD) growth on nickel foam skeletons.[1,9,21,22] Owing to low-cost and large-scale production, GOs have been extensively used as a precursor to assemble into graphene foams with macroscopic structures. However, the graphene foams prepared by this method show a low electrical conductivity because of the introduction of structural defects in the graphene basal planes during the oxidation process.[5,20,23,24] In addition, the graphene foams show a macroscopic disordered structure because of the random assembly of the reduced GO.[6,7,16−18,20] These disadvantages restrict the applications of GO-derived graphene foams. As for the CVD-growth method, the graphene networks were first deposited on the nickel foams by a precise control of reaction-gas mixture flow, and then the metal skeletons were etched to obtain graphene foams. Such method is relatively complex and not easily operated, especially for the etching process. Therefore, it still remains a challenge to develop a simple and effective route to fabricate highly conductive graphene-based foams with ordered macroscopic structures.

Herein we have developed a polymer template-assisted assembly strategy for fabricating a novel class of flexible graphene–Ag nanowire (AgNW) hybrid foams. The resulting hybrid foams show a monolith of 3D ordered networks with binary structures, in which charge carriers can pass through the defect region of graphene rapidly with the aid of the high-quality AgNW building blocks, leading to high electrical conductivity. The electrical conductivity of the hybrid foams can be up to 1028 S/m, which is near 45-fold higher than that of pure graphene foams and comparable to that of CVD-growth graphene foams.[1] The combination of high conductivity and excellent mechanical flexibility qualifies the hybrid foam applications for high performance flexible conductors. Importantly, the assembly process is conducted in aqueous solution, and the polymer templates are easily removed by a simple pyrolysis process, indicating that our approach is a facile protocol for fabricating the hybrid foams.

EXPERIMENTAL SECTION

Synthesis of Ag Nanowires (AgNWs). AgNWs were synthesized by a modified method from the reported study.[25] Briefly, 0.85 g of PVP powder was dissolved into 80 mL of glycol at 90 °C, and the mix solution was cooled down to room temperature. Then, 0.85 g of

Received: August 31, 2014
Accepted: November 7, 2014
Published: November 7, 2014

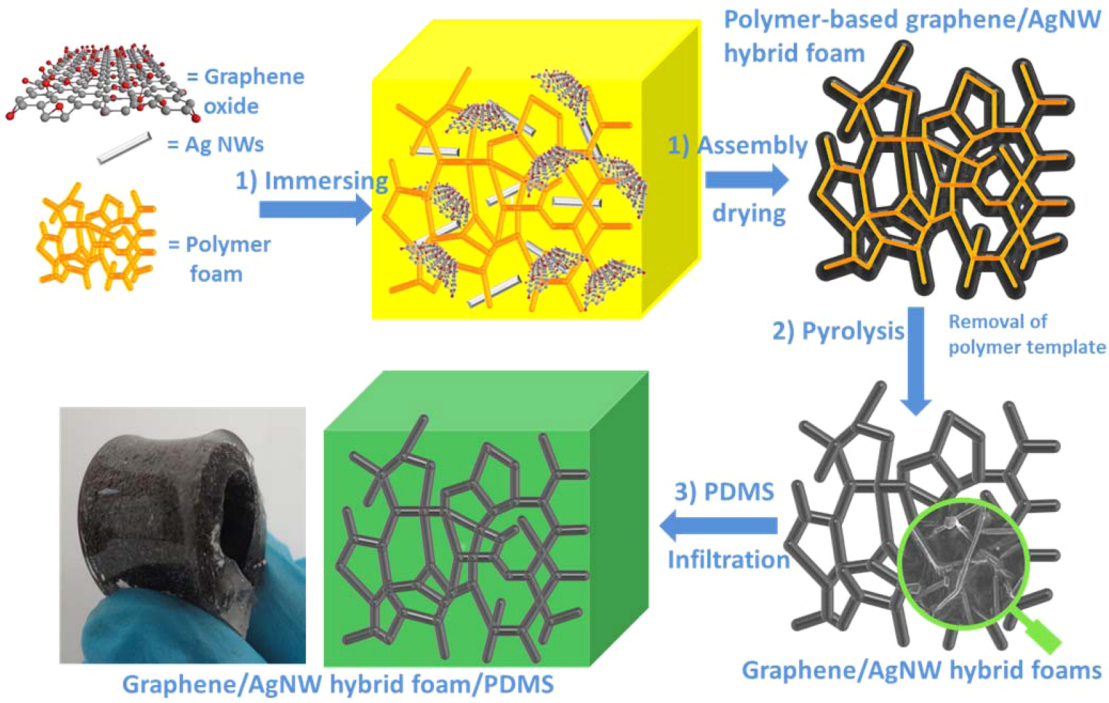

Figure 1. Fabrication process of the graphene/AgNW hybrid foams, including (1) immersion of a commercial polyurethane foam into precursor solution consisting of GO and AgNWs; (2) formation of polyurethane-based graphene/AgNW hybrid hydrogels by in situ reduction of GO; (3) dry and pyrolysis of the polymer-based hybrid gels to result in the desired graphene/AgNW hybrid foams; (4) infiltration of polydimethylsiloxane (PDMS) into a hybrid foam to obtain a flexible conductor.

$AgNO_3$ and 0.85 mg of $CuCl_2{\cdot}2H_2O$ powder were added into 10 mL of glycol, respectively. Afterward, the obtained $CuCl_2{\cdot}2H_2O$ glycerol solution was added into the PVP solution and the mixture heated up to 160 °C under gentle stirring (~50 rpm). Subsequently, the obtained $AgNO_3$ solution was added dropwise into the above mixture solution by dropping funnel. After reaction for 2 h at 160 °C, the desired AgNWs were obtained by centrifugation separation and washed with DI water. They are stored in water solution for later use.

Fabrication of Graphene/AgNW Hybrid Foams via a Polymer-Assisted Assembly Method. In a typical process, a commercially available polyurethane foam with macroporous structure was cleaned by DI water for several times, followed by completely drying at 80 °C for 2 h. Then, the clean polymer foam was cut into small pieces with length by width by thickness of 4 × 1.5 × 0.3 cm^3. All the foam pieces were immersed into the aqueous solution containing GO (~7 mg/mL), AgNWs (~15 mg/mL), and dopamine (0.1 mg/L), then picked out and transferred into a 50 mL Teflon vessel. The dopamine is utilized for reduction of GO in the following process. Compared to traditional reduction agent (hydrazine), dopamine is environmentally friendly and has low toxicity. Second, the vessel was closed, placed in an oven, and heated to 100 °C. After reaction for 12 h, a monolithic gel-like product was taken out from the vessel and directly dried to obtain the polymer-based graphene/AgNW hybrid foams. After pyrolysis of the obtained polymer-based hybrid foams at 700 °C for 2 h in nitrogen atmosphere, the desired graphene/AgNW hybrid foams were achieved. The resulting hybrid foams show a density of ~18 mg/cm^3, which corresponds to a porosity of ~99.7 vol %. The volume ratio of graphene/AgNW for the hybrid foams can be adjusted by controlling the concentration of GO and AgNWs in the precursor solution.

Preparation of the Hybrid Foam/Polydimethylsiloxane (PDMS) Composites. The hybrid foam composites were fabricated by infiltrating the free-standing hybrid foams with PDMS prepolymer, a mixture of base and curing agent with a mass ratio of 10:1, followed by degassing in a vacuum oven for 30 min and thermally curing at 80 °C for 5 h.

Characterization. The morphology and microstructure of the samples were investigated by FE-SEM (nanoSEM 230, NOVA), TEM (JEM-2010, JEOL, Japan), XRD (D/max-2200/PC, Rigaku, Japan), and Raman (LabRam HR800, Jobin Yvon, France). Thermogravimetric analysis (TGA-209F3, NETZSCH, Germany) was carried out under a 20 mL/min N_2 purge at a heating rate of 10 °C/min from room temperature to 800 °C. The real-time electrical resistance variations of the samples were measured by a two-point device under mechanical deformation. In this measurement, two copper wires were embedded and connected to the hybrid foams with silver paste before infiltration with monomers of PDMS, which enables a strong contact at the junctions. Every electromechanical experiment was repeated 5 times, and the value of electrical resistance is the average value. The electrical conductivity of the samples was also measured by a four-probe instrument (PZ-158A-SB118, Qianfeng, China). The morphology change of the hybrid foam scaffold was observed by optical microscopy. The hybrid foam/PDMS composites were cut into a thin sheet sample (3 cm × 1 cm × 1 mm), and then the sample was stretched to a set strain by a tensile machine. At this stretching state, the sample was fixed a glass slide, and then taken down for observation in the microscopy. Afterward, the sample was taken down from the glass slide, and the same process was used to observe the morphology change of the hybrid foam scaffold at a larger strain of the sample.

RESULTS AND DISCUSSION

The overall fabrication process of the graphene/AgNW hybrid foams and their integration with polydimethylsiloxane (PDMS) rubber are illustrated in Figure 1. The commercial polyurethane foam, a 3D interconnected scaffold with porous structure, serves as the template to support hybrid foam because it is easily available. After the polymer foam is dipped into GO and AgNWs solution with dopamine by a squeezing and vacuum degassing procedure, GO would be reduced into graphene sheets by dopamine, leading to a 3D monolithic graphene/AgNW hydrogel, with a color change from yellow-white to

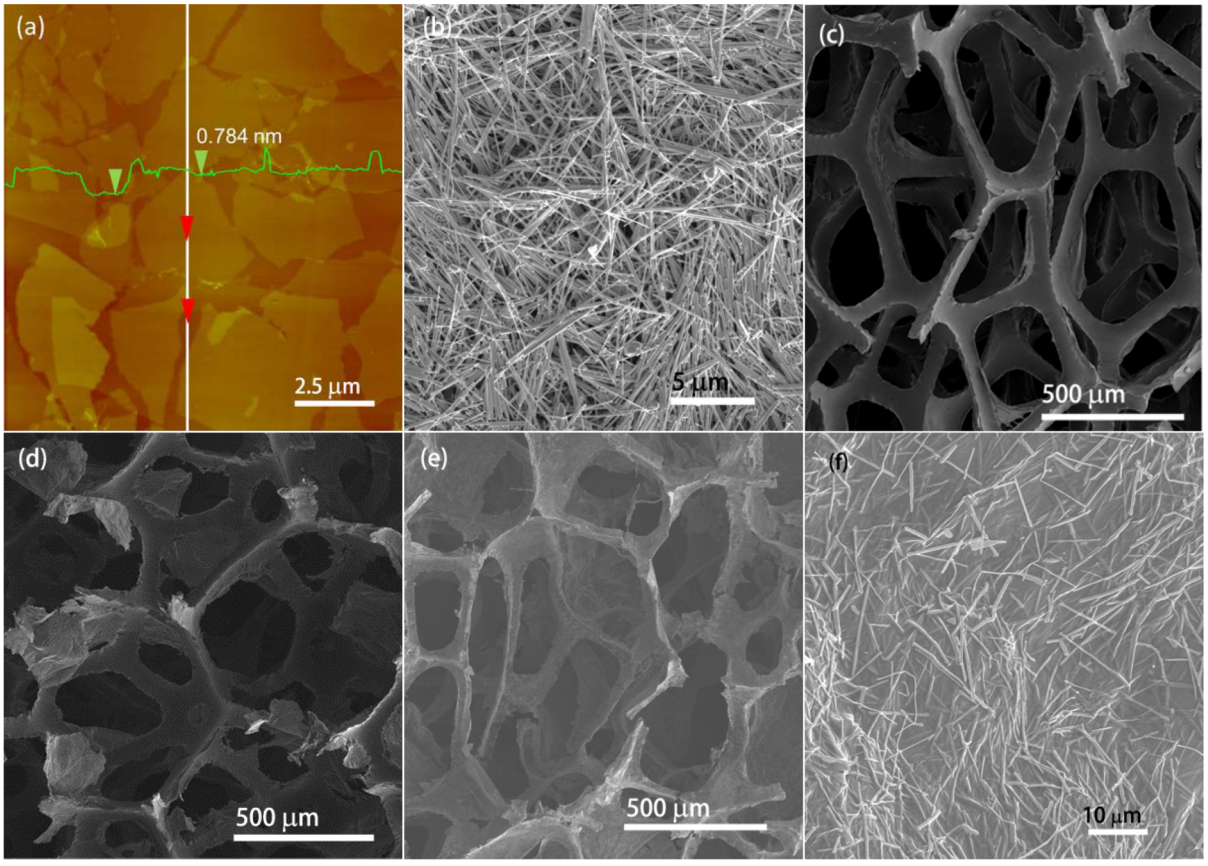

Figure 2. (a) AFM image of GO sheets. (b) SEM image of AgNWs. SEM images of (c) polyurethane foam, (d) polymer-based graphene/AgNW hybrid foams, and (e) the obtained hybrid foams after removal of polymer-templates. (f) Magnified SEM image of the hybrid foam skeletons.

black. Finally, the resulting monolithic hydrogel was dried and pyrolyzed to result in continuous and interconnected hybrid foams. Because the polymer template has much lower thermal decomposition temperature in comparison with graphene and AgNWs, it can be easily removed by the pyrolysis process. In addition, the reduction level of GO and the interfacial junction between graphene and AgNWs can be enhanced.

GO shares the same 2D framework structure with graphene, but bears hydroxyl and epoxide functional groups on its basal plan.[26] Supporting Information Figure S1 shows XRD patterns of GO and graphite. A substantial shift of the diffraction peak (002) is observed from graphite to GO because a large number of oxide-containing groups are intercalated into graphite layers during the oxidation process. The presence of these functional groups facilitates GO dispersion in water and other polar organic solvents. After spinning a coating of GO solution on a mica plate, the GO morphology was elucidated by atomic force microscopy (AFM). A typical AFM image (Figure 2a) reveals many free-standing sheets with the size of several micrometers, and their thickness is about 0.78 nm, consistent with previous study.[27] The large aspect ratio and excellent dispersion enable GO to form liquid crystals in aqueous solution. Figure 2b shows a scanning electron microscopy (SEM) image of AgNWs. Their length is about 10−20 μm with ∼300 nm in the diameter (Supporting Information Figure S2). AgNW building blocks were synthesized under the presence of polyvinylpyrrolidone (PVP) ligands, and thus, the resulting AgNWs are coated by PVP chains, which can form the hydrogen-bonding with the functional groups of GO. Therefore, GO can improve the dispersion of AgNWs, consistent with the result of previous study.[28] As shown in Supporting Information Figure S3, the GO/AgNWs mixed solution does not show obvious layering after storage for 12 h.

The morphology and structure of the as-prepared hybrid foams were investigated by SEM. Figure 2c−f displays the typical SEM images of the hybrid foams obtained by 700 °C annealing treatment. An interconnected, porous 3D network was observed. The 3D porous structure of the hybrid foams is similar to that of polymer foams, indicating that the hybrid network still remains a 3D scaffold although the polymer skeletons have been removed by the high temperature annealing treatment. Notably, compared to the original polymer foams and the CVD-growth foams, there exist some large hybrid sheets connected on the skeleton of hybrid foams, which enable them to offer larger surface area within a unit volume. A magnified SEM image of the hybrid foams shows that randomly oriented individual AgNWs are uniformly distributed between graphene layers, indicating that AgNWs remain in their original shape after the annealing process. The hybrid foams were collected and pressed into disk-like paper for XRD analysis, as shown in Supporting Information Figure S4. Compared to the graphene sheets, the peak (002) intensity of hybrids sharply reduces, indicating that the restacking of graphene into a layer structure is inhibited by the AgNWs. This result further confirms that the AgNWs have been inserted into the graphene layers. The content of AgNWs could be easily tuned by simply adjusting the ratio of GO to AgNWs in the fabrication process. Supporting Information Figure S5 shows the SEM images of hybrid foams with various graphene loading.

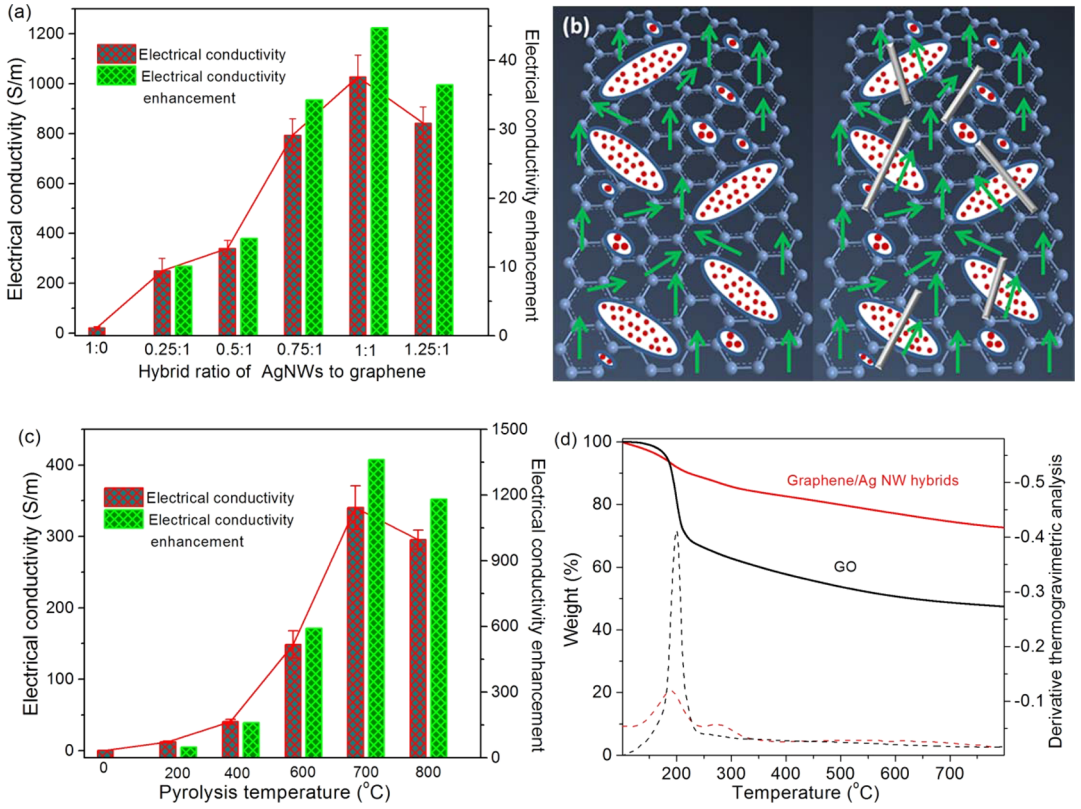

Figure 3. (a) Electrical conductivity variation of the hybrid foam as a function of the AgNW/graphene hybrid ratio. (b) The schematic figure for interpreting the resistance of graphene and AgNW hybrids, where red dots, green arrows, and gray rods represent oxygen-rich defect regions, current directions, and AgNWs, respectively. (c) The temperature-dependent conductivity for the hybrid foams with a volume ratio of AgNWs to graphene (0.5:1). (d) TGA curves of GO and the graphene/AgNW hybrids.

Table 1. Electrical Conductivity of Graphene Films[a]

sample name	form	electrical conductivity	ref
graphite	pellet	8.45×10^4 S/m (air-dried)	32
chemically converted graphene (HI-AcOH)	pellet	3.04×10^4 S/m (air-dried)	32
chemically converted graphene	free-standing paper	7.2×10^4 S/m (air-dried)	33
		3.5×10^4 S/m (dried at 500 °C)	
CVD-grown graphene	free-standing paper	1.09×10^5 S/m	34
Ag-doped graphene	fiber	9.3×10^4 S/m	28
graphene/Ag nanoparticles hybrids	free-standing paper	4.9×10^4 S/m	present work
graphene/AgNWs hybrids	free-standing paper	6×10^5 S/m	present work

[a]The graphene/AgNW and graphene/Ag nanoparticle ratios are both 1:1 in this study.

More AgNWs are inserted into the hybrid skeletons with increasing the ratio of Ag to GO.

The resulting graphene/AgNW hybrids are further investigated by thermal gravimetric analysis (TGA) and Raman spectra. One can see from Supporting Information Figure S6 that the TGA curve of the hybrids provides a quantitative analysis of the residual groups. It reveals a minor mass loss (5.7%) of the groups while GO shows a large mass loss of (52.5%) at 800 °C, suggesting that most of the oxygen-containing groups have been removed during the chemical reduction and pyrolysis process. Raman technology provides further evidence for the GO reduction. As shown in Supporting Information Figure S7, GO exhibits two strong major bands, the G-band at around 1580 cm^{-1} and D-band at around 1345 cm^{-1}, which originate from the E_{2g} mode of the aromatic carbon rings and disorders of defects, respectively.[29,30] Compared with GO, the G band of the hybrids shifts to a low-wavelength direction, indicating that the conjugated region is restored. However, the similar intensity of D and G bands reveals that the graphene sheets in the hybrids still have structural defects despite the restoration of the conjugated region.[31]

The free-standing hybrid foams show low weight and extremely high electrical conductivity. For example, the hybrid foams with a volume ratio of AgNWs to graphene (1:1) have a density of ~18 mg/cm^3, which corresponds to a high porosity of ~99.7%. As shown in Figure 3a, their electrical conductivity is up to 1028 S/m, which is comparable to that of previously reported CVD-growth graphene foams.[1] In order to measure the intrinsic conductivity of the skeleton of hybrid foams, we utilized a similar method to prepare a hybrid films. The cross-section of one film is shown in Supporting Information Figure S8. Table 1 summarizes the electrical conductivity of the graphene films reported in the literature. One can see that our

hybrid film shows high conductivity of 6×10^5 S/m, which is much higher than that of previously reported graphene films or graphene fibers. Such superior conductive performances can certainly be attributed to the synergistic effect of the 2D flexible graphene sheets and the 1D AgNWs. For comparison, the pure graphene foams were fabricated by the same method. The resulting foams show an electrical conductivity value of only ~22.5 S/m, much lower than that of the hybrid foams. Currently, the detailed structure of GO and GO-derived graphene are still not clear. Hirschmugl et al.[35] and Grossman et al.[36] demonstrated that GO structures undergo a phase transformation into oxygen-rich and graphitic (oxygen-poor) regions by thermal-driving during the reduction process. Oxygen-rich defect regions show a semiconducting behavior with a band gap of ~0.9 eV.[35] The formation of highly resistive oxygen-rich domains may lead to the carriers being trapped periodically in domains. Thus, like the grain boundary (GB) defects of CVD-grown graphene,[37] Oxygen-rich domains in GO-derived graphene may be the major defects at the interfacial regions between two graphitic domains. Jeong et al.[38] theoretically predicted that the detrimental effect of GB defect domains can be eliminated through the introduction of 1D metal NWs on the 2D graphene surfaces. In this study, many of the AgNWs were inserted between graphene layers to bridge the oxygen-rich domains for connecting the graphitic regions, resulting in the electrical connection the graphitic regions and thus leading to a high electrical conductivity of hybrid foams, as shown in Figure 3b. For comparison, Ag nanoparticle/graphene hybrid foams were also fabricated by the same method, and their electrical conductivity is nearly equal to that of pure graphene foams (Supporting Information Figure S9). The conductivity of hybrid foams is related to the volume ratio of AgNWs to graphene. The AgNWs and graphene exhibit synergistic effects on the electrical transport, resulting in the electrical conductivity of hybrid foams not showing a monotonic increase with the increase of AgNW/graphene ratios in the skeletons. In this case, there exists an optimal AgNW/graphene ratio (1:1) for the maximum conductivity, which is 45-fold higher than that of pure graphene foams (Figure 3a).

Figure 3c shows an annealing temperature-dependent electrical conductivity of the hybrid foams, which demonstrates that graphene plays an important role in determining the conductivity and provides a further evidence for illustrating the synergistic effects between graphene and AgNWs. The unannealed hybrid foams show a very low conductivity of only 0.25 S/m because of the low reduction level for GO-derived graphene. This value is close to that of the unannealed graphene foams, indicating that the AgNWs do not form percolation networks in the skeletons of the unannealed hybrid foams. After 2 h annealing at 400 °C, the obtained hybrid foams show a conductivity enhancement of 161-fold in comparison with the unannealed foams. Such an enhancement should be attributed to both the higher reduction level of graphene and the decomposition of PVP coated around the AgNWs. As shown in Figure 3d, there exists a small mass loss corresponding to the pyrolysis of PVP near 300 °C, leading to a lower junction resistance between graphene and AgNWs. However, as the annealing temperature is improved beyond 600 °C, the conductivity enhancement of hybrid foams is up to 1361-fold, much higher than that in the case at 400 °C (161-fold). Considering the facts that percolative networks of AgNWs in the unannealed hybrid system do not exist and that the high temperature annealing process causes phase segregation of the GO-derived graphene, we attribute the significantly enhanced conductivity to the bridging effects of the AgNWs between the disordered defect regions.

Three-dimensional conductive networks have showed many attractive practical applications.[18,39,40] One is to fabricate high performance polymer composites depending on their superior properties.[41] In this study, we fabricate the hybrid foam/PDMS composites by impregnating the hybrid foams with PDMS. The resulting composites show excellent mechanical flexibility including bending, stretching, and twisting, as shown in Supporting Information Figure S10. After releasing the loading, they can completely recover their original shape without mechanical failure. In addition, the hybrid foam composites also display a high electrical conductivity. For example, the composite samples with 0.3 vol % graphene/Ag (1:1) hybrid foam have a very high conductivity of up to 1000 S/m, which is comparable to that of original hybrid foam (1028 S/m), indicating that the introduction of PDMS matrix does not destroy the interconnected 3D framework of the hybrid foams. Table 2 summarizes the electrical conductivity of polymer-based graphene composites reported in the literature and the present research. One can see that the conductivity value of our composites is about several orders of magnitude higher than that of polymer-based graphene and carbon nanotube (CNT) composites with the same filler loading fraction.[1,42−49] Although these reported composites have the conductive percolative networks consisting of fillers, there exists a high junction resistance between conductive fillers in the 3D percolation networks, along with low intrinsic conductivity for fillers, leading to a low electrical conductivity for the composites.

Table 2. Electrical Conductivity of Polymer-Based Graphene Composites

polymer matrix	type of filler	filler content	electrical conductivity	ref
polystyrene	functionalized graphene	2.5 vol %	1 S/m	43
polystyrene	functionalized graphene	4.19 vol %	4.19 S/m	44
polycarbonate	functionalized graphene	2.2 vol %	51.2 S/m	45
cellulose	graphene	~4.8 vol %	71.8 S/m	46
polyurethane	graphene	~4.8 vol %	30 S/m	47
chitosan	graphene	~2.2 vol %	1.2 S/m	48
polystyrene	functionalized graphene	~2.0 vol %	~2 S/m	49
epoxy resin	graphene sponge	~0.9 vol %	~0.21 S/m	23
PDMS	CVD-grown graphene foam	~0.22 vol %	~1000 S/m	1
PDMS	graphene/AgNW hybrid foam	~0.3 vol %	~1000 S/m	present work

The hybrid foam composites exhibit not only high electrical conductivity but also excellent mechanical flexibility, which render the composites great potential for flexible and stretchable conductors,[50−52] a key component of flexible electronic devices such as artificial skins,[53] flexible sensors and actuators,[54,55] and wearable communication devices.[40,56,57] In the following, we further investigated the resistance variation of the composite with 0.3 vol % hybrid foams under bending and stretching deformation. Figure 4a shows the resistance (R)

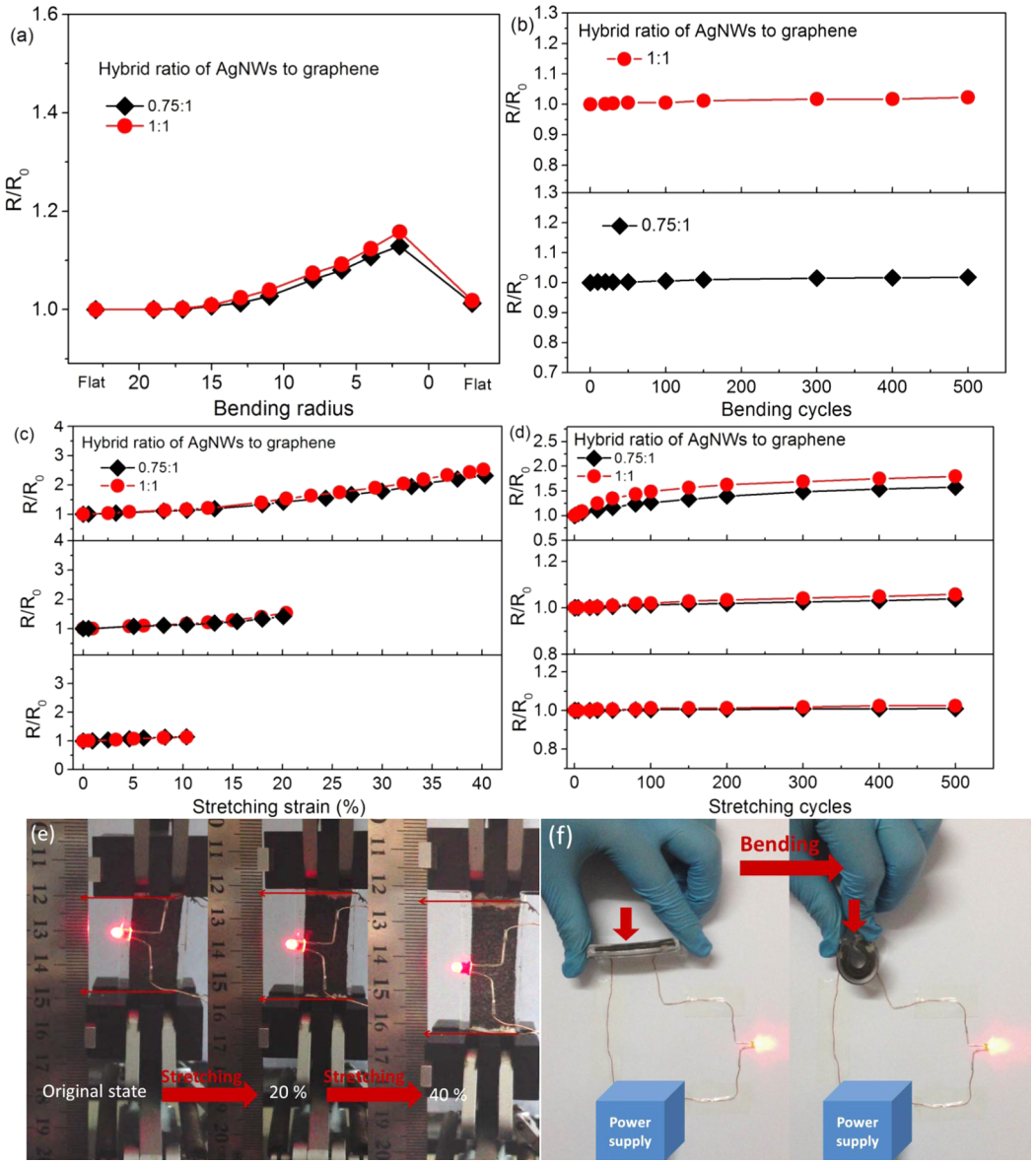

Figure 4. Electrical resistance variation of the hybrid foams composites under a mechanical deformation. (a) Electrical resistance variation of the composites with increasing the bending radius up to 2 mm. (b) Electrical resistance variation of the composites as a function of cycles for a bend radius of 2 mm. (c) Electrical resistance variation of the composites when being stretched to a set strain (10%, 20%, and 40%) and then being recovered for cycles. (d) Electrical resistance variation of the composites as a function of cycles for a set strain. (e, f) Optical images of the LED lights under the bending and stretching of the composites. The hybrid foam loading of the composites is about 0.3 vol %.

evaluation as a function of bending radius (r). R_0 represents the original resistance of the composites before testing. The normalized electrical resistance (R/R_0) shows a slight variation until r reaches 10 mm, and then gradually increases to 1.16 as the bend radius increases up to 2 mm for the composites with a AgNW/graphene ratio (1:1). Upon straightening, the resistance returns to the original values. Notably, the resistances of the composites are still very stable with an increase of bending–unbending cycles, showing a very small variation of <2.5% after 500 cycles (Figure 4b). Such results demonstrate the excellent electromechanical stability of hybrid foam/PDMS composites, which is comparable to that of CVD-grown graphene foam[1,13] and metal foam composites.[39]

The stretching strain (ε) dependence of the electrical resistance is given in Figure 4c. Similar to the results in the bending tests, the normalized resistance (R/R_0) of the hybrid foam (the AgNW/graphene ratio is 1:1) composites is nearly invariable under 10% stretching, and then gradually increases to 1.5 under 20% stretching, to 2.5 under 40% stretching. The resistance cycle performance of the composites depends on the stretching strains. Under the larger strain, more cycles are required for the hybrid foam conductors to reach stable state (Figure 4d). The electromechanical properties of the hybrid foam composites under stretching are superior to those of the elastic conductors based on Ag flake-CNT hybrid films,[58] highlighting the great potential for stretchable conductors. The rupture strains of the hybrid foam composites with the AgNW/graphene ratio of 0.75:1 and 1:1 are up to 54% and 52%, corresponding to the normalized resistance (R/R_0) of 3.1 and 3.5, respectively (Supporting Information Figure S11). The rupture strain is relatively lower than that (90%) of the graphene foam-based composites, which is ascribed to the

following two reasons. One is that AgNWs reduce the flexibility of graphene foams. In addition, large hybrid sheets connected on the skeleton of hybrid foams reduce the continuation of PDMS matrix. The hybrid foam composites with the hybrid ratio of AgNWs to graphene (1:1) show a larger resistance variation in comparison with the composites with the hybrid ratio of 0.75:1. Such a phenomenon might be attributed to the hybrid structure of the foam skeletons. With increasing the hybrid ratio, more junctions between AgNWs and graphene form, and thus more junctions could loosen during the stretching process, leading to larger resistance variation.

In order to understand the function of hybrid foam framework for the stretchable conductors, we further investigated the framework structure deformation of the composites by an optical microscopy during the stretching process. As shown in Supporting Information Figure S12, as the stretching strain increases from 0 to 30%, the skeletons of the hybrid foams elongate in the direction of the tensile force without breaking, demonstrating the excellent flexibility. This shape deformation of the hybrid foam skeletons at the microscale under a strain guarantees a continuance of the conductive network in the PDMS, leading to the good electromechanical properties. As a proof of concept application, the hybrid foam composites sever as flexible and stretchable conductors to integrate LED lights, as shown in Figure 4e,f. The LED lights show almost no variation after stretching the conductor to a set strain of up to about 20%, or bending the conductor to a radius of 5 mm. When the strain is increased to about 40%, the LED light only displays tiny change because of a resistance increase of the hybrid foam conductors.

CONCLUSIONS

In summary, a novel class of graphene/AgNW hybrid foams has been developed by polymer template-assisted assembly technique. Graphene sheets and AgNWs sever as building blocks to interconnect into a 3D flexible network, leading to a high electrical conductivity comparable to CVD-grown graphene foams. The hybrid foams show 3D ordered microstructures, high thermal stability, and excellent electrical and mechanical properties, giving them huge potential for applications such as supercapacitor and lithium-ion battery electrodes, elastic conductors, and electromagnetic shielding. As a promising application, the hybrid foam-based PDMS composites demonstrate superior electromechanical performances as flexible and stretchable conductors. Moreover, the polymer-template assisted assembly technique is a simple, scalable, and low-cost strategy, which is beneficial for large-scale production of hybrid foams. We believe that such a simple and effective fabrication protocol will provide a new synthesis pathway for various multifunctional graphene hybrid foam-based composites.

ASSOCIATED CONTENT

Supporting Information

XRD patterns of graphite and GO, SEM image of Ag nanowires (AgNWs), optical images of graphene oxide and AgNW solution with various storage time at room temperature, showing that the precursor solution is very stable, and XRD patterns of graphene and graphene/AgNW hybrids. SEM images of the hybrid foam skeletons with different volume ratios of AgNWs to graphene, TGA curves of GO and the graphene/AgNW hybrid foams, Raman spectra of GO, graphene foam, and the hybrid foams with different hybrid ratios, SEM image of the graphene/AgNW hybrid film, and SEM images of Ag nanoparticles and the skeleton of graphene/Ag nanoparticle hybrid foams. Optical images of the hybrid foam/PDMS composites under mechanical deformations and optical images of the hybrid foam/PDMS composites under different stretching strains. This material is available free of charge via the Internet at http://pubs.acs.org/.

AUTHOR INFORMATION

Corresponding Authors

*E-mail: xyhuang@sjtu.edu.cn.
*E-mail: pkjiang@sjtu.edu.cn.

Author Contributions

All authors have given approval to the final version of the manuscript.

Author Contributions

†These authors contributed equally to this work.

Notes

The authors declare no competing financial interest.

ACKNOWLEDGMENTS

The authors are also grateful to researchers in the instrument analysis center of Shanghai Jiao Tong University for their help in material analysis. The authors gratefully acknowledge support from the National Natural Science Foundation of China (No. 51107081, 51217117, 51477096), and the Special Fund of the National Priority Basic Research of China under Grant 2014CB239503. X.H. thanks the "SMC Young Star" scientist Program of Shanghai Jiao Tong University for the financial support. This work was also in part sponsored by the Shanghai Pujiang Program (PJ14D018, X.H.) and the Research Fund for the Doctoral Program of Higher Education (No. 20120073110031).

REFERENCES

(1) Chen, Z. P.; Ren, W. C.; Gao, L. B.; Liu, B. L.; Pei, S. F.; Cheng, H. M. Three-Dimensional Flexible and Conductive Interconnected Graphene Networks Grown by Chemical Vapour Deposition. *Nat. Mater.* **2011**, *10*, 424−428.

(2) Wu, C.; Huang, X. Y.; Wu, X. F.; Qian, R.; Jiang, P. K. Mechanically Flexible and Multifunctional Polymer-Based Graphene Foams for Elastic Conductors and Oil-Water Separators. *Adv. Mater.* **2013**, *25*, 5658−5662.

(3) Huang, X. D.; Qian, K.; Yang, J.; Zhang, J.; Li, L.; Yu, C. Z.; Zhao, D. Y. Functional Nanoporous Graphene Foams with Controlled Pore Sizes. *Adv. Mater.* **2012**, *24*, 4419−4423.

(4) Wang, X. B.; Zhang, Y. J.; Zhi, C. Y.; Wang, X.; Tang, D. M.; Xu, Y. B.; Weng, Q. H.; Jiang, X. F.; Mitome, M.; Golberg, D.; Bando, Y. Three-Dimensional Strutted Graphene Grown by Substrate-Free Sugar Blowing for High-Power-Density Supercapacitors. *Nat. Commun.* **2013**, *4*, 2905.

(5) Li, Y.; Chen, J.; Huang, L.; Li, C.; Hong, J.-D.; Shi, G. Highly Compressible Macroporous Graphene Monoliths via an Improved Hydrothermal Process. *Adv. Mater.* **2014**, DOI: 10.1002/adma.201400657.

(6) Hu, H.; Zhao, Z.; Wan, W.; Gogotsi, Y.; Qiu, J. Ultralight and Highly Compressible Graphene Aerogels. *Adv. Mater.* **2013**, *25*, 2219−2223.

(7) Zhao, Y.; Hu, C.; Song, L.; Wang, L.; Shi, G.; Dai, L.; Qu, L. Functional Graphene Nanomesh Foam. *Energy Environ. Sci.* **2014**, *7*, 1913−1918.

(8) Wei, W.; Yang, S. B.; Zhou, H. X.; Lieberwirth, I.; Feng, X. L.; Mullen, K. 3D Graphene Foams Cross-Linked with Pre-Encapsulated Fe_3O_4 Nanospheres for Enhanced Lithium Storage. *Adv. Mater.* **2013**, *25*, 2909−2914.

(9) Luo, J. S.; Liu, J. L.; Zeng, Z. Y.; Ng, C. F.; Ma, L. J.; Zhang, H.; Lin, J. Y.; Shen, Z. X.; Fan, H. J. Three-Dimensional Graphene Foam Supported Fe_3O_4 Lithium Battery Anodes with Long Cycle Life and High Rate Capability. *Nano Lett.* **2013**, *13*, 6136−6143.
(10) Dong, X. C.; Xu, H.; Wang, X. W.; Huang, Y. X.; Chan-Park, M. B.; Zhang, H.; Wang, L. H.; Huang, W.; Chen, P. 3D Graphene-Cobalt Oxide Electrode for High-Performance Supercapacitor and Enzyme-less Glucose Detection. *ACS Nano* **2012**, *6*, 3206−3213.
(11) Wu, Z. S.; Sun, Y.; Tan, Y. Z.; Yang, S. B.; Feng, X. L.; Mullen, K. Three-Dimensional Graphene-Based Macro- and Mesoporous Frameworks for High-Performance Electrochemical Capacitive Energy Storage. *J. Am. Chem. Soc.* **2012**, *134*, 19532−19535.
(12) Yao, H.-B.; Ge, J.; Wang, C.-F.; Wang, X.; Hu, W.; Zheng, Z.-J.; Ni, Y.; Yu, S.-H. A Flexible and Highly Pressure-Sensitive Graphene−Polyurethane Sponge Based on Fractured Microstructure Design. *Adv. Mater.* **2013**, *25*, 6692−6698.
(13) Chen, Z. P.; Xu, C.; Ma, C. Q.; Ren, W. C.; Cheng, H. M. Lightweight and Flexible Graphene Foam Composites for High-Performance Electromagnetic Interference Shielding. *Adv. Mater.* **2013**, *25*, 1296−1300.
(14) Bi, H. C.; Xie, X.; Yin, K. B.; Zhou, Y. L.; Wan, S.; He, L. B.; Xu, F.; Banhart, F.; Sun, L. T.; Ruoff, R. S. Spongy Graphene as a Highly Efficient and Recyclable Sorbent for Oils and Organic Solvents. *Adv. Funct. Mater.* **2012**, *22*, 4421−4425.
(15) Singh, E.; Chen, Z. P.; Houshmand, F.; Ren, W. C.; Peles, Y.; Cheng, H. M.; Koratkar, N. Superhydrophobic Graphene Foams. *Small* **2013**, *9*, 75−80.
(16) Chen, Z. X.; Dong, L.; Yang, D.; Lu, H. B. Superhydrophobic Graphene-Based Materials: Surface Construction and Functional Applications. *Adv. Mater.* **2013**, *25*, 5352−5359.
(17) Xu, Y. X.; Sheng, K. X.; Li, C.; Shi, G. Q. Self-Assembled Graphene Hydrogel via a One-Step Hydrothermal Process. *ACS Nano* **2010**, *4*, 4324−4330.
(18) Li, C.; Shi, G. Q. Three-Dimensional Graphene Architectures. *Nanoscale* **2012**, *4*, 5549−5563.
(19) Niu, Z. Q.; Chen, J.; Hng, H. H.; Ma, J.; Chen, X. D. A Leavening Strategy to Prepare Reduced Graphene Oxide Foams. *Adv. Mater.* **2012**, *24*, 4144−4150.
(20) Sun, H. Y.; Xu, Z.; Gao, C. Multifunctional, Ultra-Flyweight, Synergistically Assembled Carbon Aerogels. *Adv. Mater.* **2013**, *25*, 2554−2560.
(21) Yu, X. Z.; Lu, B. A.; Xu, Z. Super Long-Life Supercapacitors Based on the Construction of Nanohoneycomb-Like Strongly Coupled CoMoO-3D Graphene Hybrid Electrodes. *Adv. Mater.* **2014**, *26*, 1044−1051.
(22) He, Y. M.; Chen, W. J.; Li, X. D.; Zhang, Z. X.; Fu, J. C.; Zhao, C. H.; Xie, E. Q. Freestanding Three-Dimensional Graphene/MnO_2 Composite Networks As Ultra light and Flexible Supercapacitor Electrodes. *ACS Nano* **2013**, *7*, 174−182.
(23) Li, Y. Q.; Samad, Y. A.; Polychronopoulou, K.; Alhassan, S. M.; Liao, K. Highly Electrically Conductive Nanocomposites Based on Polymer-Infused Graphene Sponges. *Sci. Rep.* **2014**, *4*, 4652.
(24) Tang, G.; Jiang, Z.-G.; Li, X.; Zhang, H.-B.; Dasari, A.; Yu, Z.-Z. Three Dimensional Graphene Aerogels and Their Electrically Conductive Composites. *Carbon* **2014**, DOI: 10.1016/j.carbon.2014.05.063.
(25) Korte, K. E.; Skrabalak, S. E.; Xia, Y. Rapid Synthesis of Silver Nanowires Through a CuCl- or $CuCl_2$-Mediated Polyol Process. *J. Mater. Chem.* **2008**, *18*, 437−441.
(26) Bagri, A.; Mattevi, C.; Acik, M.; Chabal, Y. J.; Chhowalla, M.; Shenoy, V. B. Structural Evolution During the Reduction of Chemically Derived Graphene Oxide. *Nat. Chem.* **2010**, *2*, 581−587.
(27) Park, S.; Ruoff, R. S. Chemical Methods for the Production of Graphenes. *Nat. Nanotechnol.* **2009**, *4*, 217−224.
(28) Xu, Z.; Liu, Z.; Sun, H. Y.; Gao, C. Highly Electrically Conductive Ag-Doped Graphene Fibers as Stretchable Conductors. *Adv. Mater.* **2013**, *25*, 3249−3253.
(29) Zhou, Y.; Bao, Q. L.; Tang, L. A. L.; Zhong, Y. L.; Loh, K. P. Hydrothermal Dehydration for the "Green" Reduction of Exfoliated Graphene Oxide to Graphene and Demonstration of Tunable Optical Limiting Properties. *Chem. Mater.* **2009**, *21*, 2950−2956.
(30) Chang, H.; Sun, Z.; Yuan, Q.; Ding, F.; Tao, X.; Yan, F.; Zheng, Z. Thin Film Field-Effect Phototransistors from Bandgap-Tunable, Solution-Processed, Few-Layer Reduced Graphene Oxide Films. *Adv. Mater.* **2010**, *22*, 4872−4876.
(31) Kosynkin, D. V.; Higginbotham, A. L.; Sinitskii, A.; Lomeda, J. R.; Dimiev, A.; Price, B. K.; Tour, J. M. Longitudinal Unzipping of Carbon Nanotubes to Form Graphene Nanoribbons. *Nature* **2009**, *458*, 872−876.
(32) Moon, I. K.; Lee, J.; Ruoff, R. S.; Lee, H. Reduced Graphene Oxide by Chemical Graphitization. *Nat. Commun.* **2010**, *1*, 73.
(33) Park, S.; An, J.; Jung, I.; Piner, R. D.; An, S. J.; Li, X.; Velamakanni, A.; Ruoff, R. S. Colloidal Suspensions of Highly Reduced Graphene Oxide in a Wide Variety of Organic Solvents. *Nano Lett.* **2009**, *9*, 1593−1597.
(34) Chen, J.; Bi, H.; Sun, S.; Tang, Y.; Zhao, W.; Lin, T.; Wan, D.; Huang, F.; Zhou, X.; Xie, X.; Jiang, M. Highly Conductive and Flexible Paper of 1D Silver-Nanowire-Doped Graphene. *ACS Appl. Mater. Interfaces* **2013**, *5*, 1408−1413.
(35) Mattson, E. C.; Pu, H. H.; Cui, S. M.; Schofield, M. A.; Rhim, S.; Lu, G. H.; Nasse, M. J.; Ruoff, R. S.; Weinert, M.; Gajdardziska-Josifovska, M.; Chen, J. H.; Hirschmugl, C. J. Evidence of Nanocrystalline Semiconducting Graphene Monoxide during Thermal Reduction of Graphene Oxide in Vacuum. *ACS Nano* **2011**, *5*, 9710−9717.
(36) Kumar, P. V.; Bardhan, N. M.; Tongay, S.; Wu, J.; Belcher, A. M.; Grossman, J. C. Scalable Enhancement of Graphene Oxide Properties by Thermally Driven Phase Transformation. *Nat. Chem.* **2014**, *6*, 151−158.
(37) Kholmanov, I. N.; Magnuson, C. W.; Aliev, A. E.; Li, H.; Zhang, B.; Suk, J. W.; Zhang, L. L.; Peng, E.; Mousavi, S. H.; Khanikaev, A. B.; Piner, R.; Shvets, G.; Ruoff, R. S. Improved Electrical Conductivity of Graphene Films Integrated with Metal Nanowires. *Nano Lett.* **2012**, *12*, 5679−5683.
(38) Jeong, C.; Nair, P.; Khan, M.; Lundstrom, M.; Alam, M. A. Prospects for Nanowire-Doped Polycrystalline Graphene Films for Ultratransparent, Highly Conductive Electrodes. *Nano Lett.* **2011**, *11*, 5020−5025.
(39) Yu, Y.; Zeng, J. F.; Chen, C. J.; Xie, Z.; Guo, R. S.; Liu, Z. L.; Zhou, X. C.; Yang, Y.; Zheng, Z. J. Three-Dimensional Compressible and Stretchable Conductive Composites. *Adv. Mater.* **2014**, *26*, 810−815.
(40) Xu, F.; Zhu, Y. Highly Conductive and Stretchable Silver Nanowire Conductors. *Adv. Mater.* **2012**, *24*, 5117−22.
(41) Yu, Y.; Yan, C.; Zheng, Z. Polymer-Assisted Metal Deposition (PAMD): A Full-Solution Strategy for Flexible, Stretchable, Compressible, and Wearable Metal Conductors. *Adv. Mater.* **2014**, *26*, 5508−5516.
(42) Kuilla, T.; Bhadra, S.; Yao, D.; Kim, N. H.; Bose, S.; Lee, J. H. Recent Advances in Graphene Based Polymer Composites. *Prog. Polym. Sci.* **2010**, *35*, 1350−1375.
(43) Stankovich, S.; Dikin, D. A.; Dommett, G. H. B.; Kohlhaas, K. M.; Zimney, E. J.; Stach, E. A.; Piner, R. D.; Nguyen, S. T.; Ruoff, R. S. Graphene-Based Composite Materials. *Nature* **2006**, *442*, 282−286.
(44) Liu, N.; Luo, F.; Wu, H.; Liu, Y.; Zhang, C.; Chen, J. One-Step Oonic-Liquid-Assisted Electrochemical Synthesis of Ionic-Liquid-Functionalized Graphene Sheets Directly from Graphite. *Adv. Funct. Mater.* **2008**, *18*, 1518−1525.
(45) Yoonessi, M.; Gaier, J. R. Highly Conductive Multifunctional Graphene Polycarbonate Nanocomposites. *ACS Nano* **2010**, *4*, 7211−7220.
(46) Nguyen Dang, L.; Pahimanolis, N.; Hippi, U.; Korhonen, J. T.; Ruokolainen, J.; Johansson, L.-S.; Nam, J.-D.; Seppala, J. Graphene/Cellulose Nanocomposite Paper with High Electrical and Mechanical Performances. *J. Mater. Chem.* **2011**, *21*, 13991−13998.
(47) He, H.; Gao, C. General Approach to Individually Dispersed, Highly Soluble, and Conductive Graphene Nanosheets Functionalized by Nitrene Chemistry. *Chem. Mater.* **2010**, *22*, 5054−5064.

(48) Wang, X.; Bai, H.; Yao, Z.; Liu, A.; Shi, G. Electrically Conductive and Mechanically Strong Biomimetic Chitosan/Reduced Graphene Oxide Composite Films. *J. Mater. Chem.* **2010**, *20*, 9032−9036.
(49) Li, W.; Tang, X.-Z.; Zhang, H.-B.; Jiang, Z.-G.; Yu, Z.-Z.; Du, X.-S.; Mai, Y.-W. Simultaneous Surface Functionalization and Reduction of Graphene Oxide with Octadecylamine for Electrically Conductive Polystyrene Composites. *Carbon* **2011**, *49*, 4724−4730.
(50) Zhu, Y.; Xu, F. Buckling of Aligned Carbon Nanotubes as Stretchable Conductors: A New Manufacturing Strategy. *Adv. Mater.* **2012**, *24*, 1073−1077.
(51) Zhang, Y. Y.; Sheehan, C. J.; Zhai, J. Y.; Zou, G. F.; Luo, H. M.; Xiong, J.; Zhu, Y. T.; Jia, Q. X. Polymer-Embedded Carbon Nanotube Ribbons for Stretchable Conductors. *Adv. Mater.* **2010**, *22*, 3027−3031.
(52) Ge, J.; Yao, H. B.; Wang, X.; Ye, Y. D.; Wang, J. L.; Wu, Z. Y.; Liu, J. W.; Fan, F. J.; Gao, H. L.; Zhang, C. L.; Yu, S. H. Stretchable Conductors Based on Silver Nanowires: Improved Performance through a Binary Network Design. *Angew. Chem., Int. Ed.* **2013**, *52*, 1654−1659.
(53) Guo, R. S.; Yu, Y.; Xie, Z.; Liu, X. Q.; Zhou, X. C.; Gao, Y. F.; Liu, Z. L.; Zhou, F.; Yang, Y.; Zheng, Z. J. Matrix-Assisted Catalytic Printing for the Fabrication of Multiscale, Flexible, Foldable, and Stretchable Metal Conductors. *Adv. Mater.* **2013**, *25*, 3343−3350.
(54) Amjadi, M.; Pichitpajongkit, A.; Lee, S.; Ryu, S.; Park, I. Highly Stretchable and Sensitive Strain Sensor Based on Silver Nanowire−Elastomer Nanocomposite. *ACS Nano* **2014**, *8*, 5154−5163.
(55) Xu, Z.; Liu, Z.; Sun, H.; Gao, C. Highly Electrically Conductive Ag-Doped Graphene Fibers as Stretchable Conductors. *Adv. Mater.* **2013**, *25*, 3249−3253.
(56) Yan, C. Y.; Kang, W. B.; Wang, J. X.; Cui, M. Q.; Wang, X.; Foo, C. Y.; Chee, K. J.; Lee, P. S. Stretchable and Wearable Electrochromic Devices. *ACS Nano* **2014**, *8*, 316−322.
(57) Lin, L.; Liu, S. Y.; Fu, S. R.; Zhang, S. M.; Deng, H.; Fu, Q. Fabrication of Highly Stretchable Conductors via Morphological Control of Carbon Nanotube Network. *Small* **2013**, *9*, 3620−3629.
(58) Chun, K. Y.; Oh, Y.; Rho, J.; Ahn, J. H.; Kim, Y. J.; Choi, H. R.; Baik, S. Highly Conductive, Printable and Stretchable Composite Films of Carbon Nanotubes and Silver. *Nat. Nanotechnol.* **2010**, *5*, 853−857.